A range of fault slip styles on progressively misoriented planes during flexural-slip folding, Cape Fold Belt, South Africa

Åke Fagereng[a,b,*], Gregory Byrnes[a]

[a] *Department of Geological Sciences, University of Cape Town, Private Bag X3, Rondebosch 7701, South Africa*

[b] *Now at: School of Earth & Ocean Sciences, Cardiff University, Main Building, Park Place, CF10 3AT, Cardiff, United Kingdom*

Abstract

Flexural slip folds are distinctive of mixed continuous-discontinuous deformation in the upper crust, as folding is accommodated by continuous bending of layers and localized, discontinuous slip along layer interfaces. The mechanism of localized, layer-parallel slip and the stress and fluid pressure conditions at which flexural slip occurs are therefore distinctive of shear localization during distributed deformation. In the Prince Albert Formation mudstone sequence of the Karoo Basin, the foreland basin to the Cape Fold Belt, chevron folds are well developed and associated with incrementally developed bedding-parallel quartz veins with slickenfibers oriented perpendicular to fold hinge lines, locally cross-cutting axial planar cleavage, and showing hanging wall motion toward the fold hinge. Bedding-parallel slickenfiber-coated veins dip at angles from 18° to 83°, implying that late increments of bedding-parallel shear occurred along unfavorably oriented planes. The local presence of tensile veins, in mutually cross-cutting relationship with bedding-parallel, slickenfiber-coated veins, indicate local fluid pressures in excess of the least compressive stress.

Slickenfiber vein microstructures include a range of quartz morphologies, dominantly blocky to elongate-blocky, but in places euhedral to subhedral; the veins are commonly laminated, with layers of quartz separated by bedding-parallel slip surfaces characterized by a quartz-phyllosilicate cataclasite. Crack-seal bands imply incremental slickenfiber growth, in increments from tens of micrometers to a few millimeters, in some places, whereas other vein layers lack evidence for incremental growth and likely formed in single slip events. Single slip events, however, also involved quartz growth into open space, and are inferred to have formed by stick-slip faulting. Overall, therefore, flexural slip in this location involved bedding-parallel faulting, along progressively misoriented weak planes, with a range of slip increments.

---

*Corresponding author

Email address: `FagerengA@cardiff.ac.uk` (Åke Fagereng)

Keywords:
flexural slip; fold-and-thrust belts; brittle-ductile deformation; faulting; fluid pressure; hydrothermal veins

1. Introduction

Subgreenschist facies folding of sedimentary sequences is commonly achieved by flexural slip, where folding is accommodated by a combination of ductile buckling of layers and localized slip along layer interfaces (e.g. Chapple and Spang, 1974; Ramsay and Huber, 1987; Tanner, 1989; Fowler, 1996). Typically, bedding-parallel slip associated with flexural slip folding is recognized through the presence of slickenfibers or striations indicating (reverse) dip slip motion on bedding planes (Tanner, 1989; Fowler, 1996; Fowler and Winsor, 1997; Horne and Culshaw, 2001). Bedding-parallel veins, that can be demonstrated to have formed during folding, have been suggested to imply that locally and transiently, fluid pressures significantly in excess of hydrostatic were achieved (Cosgrove, 1993; Horne and Culshaw, 2001). Similarly, slickenfibers in other locations have also been suggested to record fluid pressure fluctuations (Renard et al., 2005) and fault slip at low effective stress (Fagereng et al., 2010). A hypothesis to consider is therefore that flexural slip is associated with frictional shear along weak and/or overpressured planes.

Bedding-parallel veins in flexural slip folds have not exclusively been attributed to bedding-parallel shear during folding. Bedding-parallel veins may also form in sedimentary successions by syn-sedimentary increases in fluid-pressure, caused by either thermal expansion or pore fluid expulsion during burial of low-permeability sediments (e.g. Nicholson, 1978; Fitches et al., 1986; Cosgrove, 1993). If burial is associated with vertical shortening and minor applied horizontal stresses, these veins would generally be tensile, and reflect opening direction perpendicular to near-horizontal bedding. It is, however, possible that shear-related dilation occurs on syn-sedimentary veins, for example in submarine landslides or early, soft-sediment thrusting (Cosgrove, 1993). Pre-folding shear veins would, however, differ from shear veins associated with flexural slip folding, in that flexural slip folding would tend to create veins with opposite shear sense either side of a fold hinge, and development of thickened veins (saddle reefs) at fold hinges (e.g. Ramsay, 1975; Fitches et al., 1986; Tanner, 1989; Cosgrove, 1993).

Geometry and microstructure of vein systems reflect stress and fluid pressure conditions during the fracturing and sealing processes involved in vein formation (e.g. Oliver and Bons, 2001; Collettini et al., 2006; Mittempergher et al., 2009; Bons et al., 2012; Fagereng et al., 2014). Here, we consider the geometry of flexural slip folds and the microstructure of bedding-parallel slickenfiber veins to discuss the timing of vein formation and the conditions of flexural slip. Folds in the Prince Albert Formation mudstones in the foreland basin of the Cape Fold Belt provide a natural laboratory of well-exposed structures, on which our arguments are based. The folds formed at temperatures less than 200°C (de Swart and Rowsell, 1974; Frimmel et al., 2001), and therefore record brittle-ductile deformation within the normally brittle, seismogenic crust (Sibson, 1984; Scholz, 1988). In the recently suggested continuum of fault behaviors, spanning slip velocities from aseismic creep to regular earthquakes (Peng and Gomberg, 2010), the mechanics of faulting during folding, a form of continuous-discontinuous behavior within the seismogenic zone, may be particularly useful to address the controls on localized versus distributed deformation in the upper crust.

2. Geological Setting

The Cape Fold Belt is generally thought to have formed in an Andean-type margin during subduction of the Paleo-Atlantic underneath the Gondwana supercontinent (du Toit, 1937; Lock, 1980; de Wit and Ransome, 1992), between approximately 300 and 180 Ma (Hälbich, 1992). The late Carboniferous (Pennsylvanian) to Middle Triassic Karoo basin is situated inland of the Cape Fold Belt, and interpreted as the retroarc foreland basin formed landward of the Cape Fold Belt during subduction (Fig. 1)(Catuneanu et al., 1998, 2005). Within the Karoo Basin, the Karoo Supergroup clastic sedimentary sequence unconformably overlies the Cape Supergroup. Whereas the Cape Supergroup rocks predate the formation of the Cape Fold Belt, the Karoo Supergroup was deposited syntectonically (Catuneanu et al., 1998, 2005). Here, we focus on deformation of the Prince Albert Formation, which is part of the Ecca Group of the Karoo Supergroup.

The Prince Albert Formation is the lowermost unit of the Ecca Group. The Ecca Group was deposited in the early Permian (Visser, 1990; Bangert et al., 1999), and in the southern section of the main Karoo Basin it overlies the Dwyka Group, a glacial diamictite and the oldest group of the Karoo succession (Catuneanu et al., 1998, 2005). The Whitehill Formation, a black, carbonaceous shale, overlies the Prince Albert Formation (Visser, 1992). The Prince Albert Formation is a greenish-grey, mudstone package between 40 and 300 m thick (Johnson et al., 2006), containing tuffaceous layers dated to 288 ± 3.0 Ma and 289 ± 3.8 Ma (Bangert et al., 1999). After the deposition of the Prince Albert Formation, the main Karoo Basin continued to fill concurrent with north-south shortening in the Cape Fold Belt (Hälbich, 1992;

Catuneanu et al., 2005), leading to burial and horizontal shortening of the Prince Albert Formation. Frimmel et al. (2001) investigated the metamorphic conditions in the Cape Fold Belt, and concluded that the Cape Supergroup did not experience temperatures in excess of 300°C. Because the Karoo sediments were deposited on top of the Cape Supergroup, it is likely that the Prince Albert Formation was deformed under peak low-grade metamorphic conditions between 150 and 200°C (de Swart and Rowsell, 1974).

The field area of this study is located approximately 12 km south of the town of Laingsburg, where the Prince Albert Formation crops out within the northern foreland of the Cape Fold Belt (Fig. 1). The folds in the Prince Albert Formation mudstones in this area have previously been briefly described by Fagereng (2012) who noted the presence of chevron folds and abundant bedding-parallel, slickenfiber-coated flexural slip faults (Fig. 2). Craddock et al. (2007) studied calcite twins within the Prince Albert Formation, and unraveled two distinct deformation events; one of bedding-parallel, north-south greatest shortening, and a second reflecting bedding-oblique, steeply northeast plunging greatest shortening. The first event is consistent with approximate bulk pure shear and associated upright to steeply inclined folding, whereas the second may reflect a subsequent episode of overthrusting (Craddock et al., 2007).

3. Fold Geometry

The Prince Albert Formation is characterized by chevron folding at wavelengths ranging from less than a meter to about hundred meters. Folds are defined by folded bedding and associated with an axial planar cleavage. Within the Prince Albert Formation, in the study area, bedding thicknesses are typically ~ 30 cm, but range from thin laminations (< 1 cm) to thick beds (~ 100 cm) (Fig. 2a). Beds are laterally continuous along strike for at least tens of meters, where they have not been truncated by local reverse faults. Beds can further be differentiated into more competent silt-rich, clay-poor units and more incompetent clay-rich, silt-poor units (e.g. Fig. 2b). Tuff layers are locally present and a few centimeters thick.

Bedding surfaces predominantly dip to the north-northeast and south-southwest at angles ranging from 20° to 80°, such that fold interlimb angles vary from open to tight (Fig. 3a). Fold hinge lines are sub-horizontal and plunge gently ESE and WNW (Fig. 3a). The regional fold axial plane is steeply inclined to the south-southwest, reflected by an axial planar cleavage that varies from subvertical to moderately inclined (Fig. 3a). In other words, the folds are upright to moderately inclined and approximately south verging. Pencil lineation, sub-parallel to fold hinge lines, is abundant in clay-rich layers, and formed by the intersection of bedding and axial planar cleavage. This lineation therefore approximates the orientation of the fold hinge line, and also plunges gently both ESE and WNW (Fig. 3a). Fold hinges are commonly angular, forming chevron folds, although more rounded fold hinge zones exist in more clay-rich horizons (Fig. 2a,b). Slickenlines and slickenfibers (Fig. 2c) plunge north-northeast and south-southwest at angles between 20° and 80° (Fig. 3b), and are thereby approximately orthogonal to the average ESE and WNW trending fold hinge lines (Fig. 3b). Fault planes containing the slickenfibers are generally bedding-parallel (Figs. 2a,b,3b), although in places cut upwards through bedding, particularly near fold hinges (Fig. 2a). Slickenfiber steps indicate reverse shear sense (Fig. 2c), and reversal in shear sense across fold hinges as expected in flexural slip folds.

4. Slickenfiber-Coated Veins

Bedding-parallel faults are abundant in the Prince Albert Formation and are identified from the presence of bedding-parallel slickenfiber shear veins. These veins dip at angles between 20° and 82° (Fig. 4). Some slickenfibre veins are bedding-discordant, and have dip angles in the range 18° to 83°, with a median value of 45 - 60° (Fig. 4). Single slickenfiber veins can be traced along strike for at least tens of meters. Vein thicknesses are variable both along-strike, down-dip, and between veins, but typically range from 0.5 to 20 mm.

Slickenfiber-coated veins are continuous across fold hinges of open folds with gently dipping limbs (e.g. Fig. 2b). A reverse shear sense consistent with flexural slip occurs on fold limbs on either side of fold hinges, i.e. the shear sense reverses across the hinge, and there is no sign of shear displacement at the hinge itself. Veins are commonly thickest in fold hinge zones, comparable to saddle reefs described in Horne and Culshaw (2001). Craddock et al. (2007) reported slickenfibers that do not change shear sense across the fold hinge, but we find only very rare, isolated examples of this. The examples we have found are associated with slickenfibre surfaces that cross-cut bedding, i.e. do not accommodate flexural slip folding.

The distances between consecutive shear veins along an approximately 70 m long north-south oriented outcrop transect were measured perpendicular to bedding. Figure 5a shows that there are a few distinct spikes in the cumulative distance between consecutive shear veins, which compared with field observations do not relate to thicker beds. The mean distance between shear veins is 1.2 m (s.d. = 1.3 m, n = 65), but distances range from 10 cm up to 7 m (Fig. 5b).

Slickenfibers are made up of several macroscopic quartz laminations, and are typically between 5 cm and 10 cm long (Fig. 2c,d). The generally accepted macroscopic model for forming such veins is dilation along irregularities in a fault surface, where dilational sites are filled by precipitation from a fluid (Durney and Ramsay, 1973; Gratier and Gueydan, 2007; Fagereng et al., 2010; Bons et al., 2012)(Fig. 6a). The shear veins comprise detached wallrock (mudstone) fragments, solid and fluid inclusions and sheet silicates cemented in vein quartz and in places calcite (Figs. 6b,7). In places, thicker than average shear veins, or layers within shear veins, contain mm-scale angular wallrock fragments in a matrix of vein quartz (Fig. 2d). We interpret these layers as hydrothermal breccias, but cannot confidently define them as either implosion or hydrofracture breccias. The brecciated fragments have variable shapes and orientations, but in general high aspect ratio fragments have long axes orientated subparallel to the vein walls.

5. Vein Microstructure

Photomicrographs were taken of thin sections cut parallel to slickenfibers and perpendicular to vein margins. In the following section, we discuss vein morphology and microstructure. Crack-seal band spacing, as defined by distinct bands of fluid and solid inclusions, and angles between crack-seal bands and inferred slip surfaces were measured on scaled digital photomicrographs using ImageJ software.

5.1. Internal Vein Geometry

The slickenfiber shear veins are generally composed of multiple layers of quartz and minor calcite, separated by subparallel wallrock layers or one or more cataclastic shear surfaces that are also subparallel to bedding (and thereby the vein margin) (Figs. 2d, 6a,b, 7a-d). As such, the internal geometry is consistent with type B bedding-veins as described by Koehn and Passchier (2000). The cataclasites are tens of micrometers thick surfaces, continuous for up to tens of centimeters, and characterized by fine-grained, quartz and phyllosilicate material cross-cutting vein quartz (Fig. 7c,d). Because the veins reflect bedding-parallel shear, wallrock layers parallel to the vein margin (e.g. Fig. 7a) must have been the bedding surface at some point in time, and can therefore also be interpreted as a slip surface. Consequently, the vein margin-parallel surfaces that define the internal layering of the shear veins are interpreted as localised shear surfaces, and referred to as such. These shear surfaces are comparable to the 'micro-transforms' defined by Fagereng et al. (2010) in slickenfiber veins from the Chrystalls Beach Complex.

The overall geometry of the slickenfiber veins is a laminated structure where laminae are separated by shear surfaces (Fig. 6). In the classic growth model for slickenfiber veins, this structure is achieved by slip on the shear surfaces, associated dilation in microscopic dilational jogs, and slickenfiber growth as the dilational sites fill with a precipitate, in this case mostly quartz with minor calcite (Fig. 6a). In the event that slip on the shear surfaces is episodic, crack-seal inclusion bands (Ramsay, 1980) may develop (Fig. 6a). Where crack-seal bands are clearly observed, those that lie along the same shear surface are subparallel and mimic the shape of the wallrock-slickenfibre interface at the end the shear surface. Shear surfaces are typically at an angle of 50° to 70° to crack-seal bands and extension veins (Figs. 6b, 7a,b,d). Because crack-seal bands form during slickenfibre growth, this must be the original angle between shear surfaces and inclusion bands, and any subsequent rigid body rotation would not alter this angle. If the folds were unfolded, the inclusion bands would dip toward antiform hinges. This is consistent with a reverse shear sense of slickenfibre veins formed during flexural slip folding, as also inferred by Fowler (1996) in chevron folds in Bendigo-Castlemaine, Australia.

The microscopic structure of individual vein layers is controlled by several parameters, including stress, fluid pressure, temperature, Peclet number (diffusive vs. advective material transport), fracture opening rate, precipitation rate, among others (e.g. Durney and Ramsay, 1973; Oliver and Bons, 2001; Bons et al., 2012, and references therein). We therefore describe the quartz morphology within slickenfibers in the next subsection.

5.2. Quartz Morphology

Quartz is the dominant vein mineral, and quartz crystal sizes vary from < 10 μm to ~ 2 mm. The dominant crystal shape is blocky to elongate-blocky grains of variable size (Fig. 7c-e), although 'stretched' crystals (*sensu* Bons et al., 2012) are significant in some places (Fig. 7f). Stretched and elongate-blocky crystals typically exceed 0.5 mm in their longest dimension, commonly have serrated grain boundaries and long axes oriented at low angles ($< 45°$) to slip surfaces (Fig. 7f). The slickenfibers therefore do not have a fibrous (sensu Bons et al., 2012) microstructure, but are rather composed of smaller aspect ratio quartz crystals. Except locally in some vein layers (Fig. 7f), quartz long axes do not have a clear preferred orientation relative to the shear surface (Fig. 7c,e). As in bedding-veins described by Koehn and Passchier (2000), quartz crystals do therefore not necessarily track vein opening, although internal layering does.

A range of quartz microstructures are exhibited in close proximity to each other, typically separated by a shear surface or set of shear surfaces (Fig. 7c-f). In places, quartz laminae with different morphology are separated by a zone containing multiple shear surfaces enveloped by a thicker cataclastic damage zone (Fig. 7c). Such cataclastic zones also separate quartz- and calcite-dominated laminae (Fig. 7d).

In places, quartz layers contain isolated wallrock fragments, which are bounded by irregular surfaces (Fig. 7a,b), and enveloped by blocky vein quartz. Wallrock is also incorporated into veins along solid and fluid inclusion bands (Fig. 7b,c,f). In places, these wallrock fragments contain a cleavage, implying they were incorporated after formation of the axial planar cleavage. Where inclusion bands are present, they indicate a crack-seal microstructure, and are commonly associated with serrated grain boundaries (Fig. 7f). However, there are numerous examples of where inclusion bands, and thus a crack-seal structure, are not present (e.g. 7d,e).

5.3. Inclusion Band Geometry

The inclusion bands are oriented at a high angle to wallrock cleavage, and mimic the shape of adjacent vein margins (Fig. 7a). Adjacent inclusion bands are subparallel, and inclined at between 30° and 80° (typically 50° to 70°) to adjacent slip surfaces (Fig. 7b,c,f). Inclusion bands are straight in places, but also curve or turn (Fig. 7a,f), although inclusion bands along the same slip surface are typically parallel. Inclusion bands tend to be continuous across single quartz layers. In places, however, inclusion bands may be discontinuous and stop at a quartz grain boundary. Within the same vein, inclusion bands may be present in only parts of one or more vein laminae.

The spacing between adjacent crack-seal inclusion bands is a measure of minimum vein opening in each crack episode (Ramsay, 1980; Renard et al., 2005; Fagereng et al., 2011). To quantify inclusion band spacing, spacings were measured along five transects, parallel to slip surfaces, in four vein samples (Fig. 8, Table 7). The number of adjacent inclusion bands varies from 17 to 165 in these transects, but it is common to find less than 17 adjacent bands in slickenfiber vein samples from flexural-slip folds in the Prince Albert Formation. The cumulative spacing between the inclusion bands reaches up to 17 mm, the entire length of a small slickenfiber (Fig. 8).

For each transect, cumulative inclusion band spacing and inclusion band number (numbered sequentially from one end of the transect to the other) show a near-linear relationship, although there are some clear steps in places (Fig. 8). The standard deviation of the inclusion band spacing is between approximately 50 and 100 % of the mean (Table 7), an effect of some spacings being significantly larger than the mean, and observed as steps in the cumulative spacing plots (Fig. 8). The mean spacing ranges from 9 μm to 1 mm, a variation of over two orders of magnitude between five transects. Four out of five transects, however, have mean spacings in the range of 9 μm to 40 μm. All the transects considered have a positively skewed frequency-spacing distribution (Fig. 8). These distributions also highlight some large deviations from the mean spacing, reflected in the significant standard deviations in all transects.

6. Discussion

6.1. Deformation History and Frictional Reactivation in the Prince Albert Formation

Hinge lines plunging gently east and west, and steeply dipping fold axial planes indicate that the studied part of the Karoo foreland basin experienced horizontal north-south shortening. Prevalent reverse dip-slip faulting on east-west striking faults indicates a regime of subhorizontal, north-south oriented, greatest compression. Assuming Andersonian mechanics, and defining the three principal compressive stresses as $\sigma_1 \geq \sigma_2 \geq \sigma_3$, this deformation regime is associated with a subvertical σ_3, and σ_2 parallel to fold hinge lines. The presence of pencil lineation formed by cleavage-bedding intersection in clay-rich units, implies that temperature was not sufficient to allow shortening-related, axial planar cleavage to become a more developed fabric than bedding ('early deformation stage' of Ramsay and Huber, 1983). This is consistent with temperature estimates by Frimmel et al. (2001), who suggest that metamorphism in the foreland of the Cape Fold Belt did not exceed subgreenschist conditions.

Slickenfiber-coated bedding-parallel veins in the Prince Albert Formation indicate that flexural slip occurred along bedding surfaces. The fact that slickenfibers trend north and south, show a reverse sense of shear, and are oriented subperpendicular to fold hinge lines implies that slickenfiber shear veins accommodated north-south shortening in the same kinematic regime as the folds. Moreover, in fold hinge zones the slickenfibre veins show a reversal in shear sense, no shear displacement at the hinge line, and significantly thickened veins, observations that put together support a syn-folding origin (cf. Fowler, 1996; Horne and Culshaw, 2001). Shear veins cross-cut wallrock cleavage (Fig. 7b), and therefore the timing of shear vein formation progressed into late stages of folding, coinciding with or post-dating the development of axial planar cleavage.

The optimal angle for frictional reactivation of a cohesion-less plane is $\theta_r^* = 0.5\tan^{-1}(1/\mu_s)$ (Sibson, 1985), measured from σ_1 in the $\sigma_1\sigma_3$ plane, and where μ_s is the static coefficient of friction. The Prince Albert Formation is composed primarily of quartz and clay minerals, and μ_s is therefore likely in the range 0.3 to 0.6 (Byerlee, 1978; Morrow et al., 1992). As a result, the optimal reactivation angle is between 30° and 37°. The stress ratio σ_1/σ_3 required for reactivation is at its lowest when the angle θ_r between the plane to be reactivated and σ_1 is equal to θ_r^* (Sibson, 1985, 1990). The required σ_1/σ_3 ratio increases significantly at angles less or more than θ_r^*, so that σ_1/σ_3 required for reactivation is ~ 50 % greater at angles $\pm$ 15° from θ_r^*, compared to at θ_r^* (Sibson, 1990). Thus, assuming σ_1 is horizontal for reverse faulting along bedding planes in the Prince Albert Formation, flexural slip is most likely to occur along beds dipping at angles between 15° and 52°. At θ_r greater than $2\theta_r^*$, reactivation can only occur if σ_3' is less than zero, where $\sigma_3' = \sigma_3 - P_f$ and P_f is fluid pressure (Sibson, 1985). Therefore, unless fluid pressure is elevated to values in excess of σ_3, bedding-parallel slip cannot occur at dip angles greater than approximately 74°.

No faults dipping at less than 15° were observed in this study (Fig. 4). Combined with the observation that slickenfiber veins in places cross-cut axial planar cleavage, this may imply that folding by flexural slip initiated only after some steepening of bedding planes had occurred by other folding mechanisms. Alternatively, continued folding after initiation of flexural slip may have led to steepening of all flexural slip faults, such that no very gentle dip angles ($< 15°$) have been preserved. These options are difficult to separate; however, it is mechanically easier to explain the evolution of flexural slip folds if at least a small amount of bending occur by early, gentle folding without bedding-parallel slip.

The average dip angle of bedding-parallel slickenfiber veins accommodating flexural slip folding is $50° \pm 14°$ (n = 58), greater than expected from the predicted optimal reactivation angle of 30° to 37° in a quartz and clay dominated sequence. Some bedding-parallel faults are also present at angles greater than the inferred lock-up angle of $2\theta_r^* = 74°$, reaching dip angles in excess of 80°. Because bulk horizontal shortening will lead to steepening of planes striking perpendicular the direction of greatest shortening, i.e. bedding on fold limbs in relatively upright folds, it is possible that progressive folding led to steepening of bedding-parallel faults also after they stopped being active. For example, the formation of a subvertical, axial planar cleavage would have contributed to horizontal shortening and associated steepening of bedding planes. However, the prevalence of bedding-parallel fault dip angles greater than the optimal reactivation angle, the observation that steeply dipping bedding-parallel faults cross-cut cleavage, and lack of deformation of vein material in fold hinges, implies that flexural slip folding occurred during progressive flattening and was in later stages of folding accommodated on faults that were steeper than the optimal reactivation angle. The range of preserved dip angles in bedding-parallel slickenfiber veins may therefore preserve a range of fault orientations from well oriented to severely misprinted, developed during progressive folding where tighter folds required slip on severely misprinted planes toward the end of folding.

A likely deformation sequence involves initiation of flexural slip folding by slip on bedding surfaces after bulk shortening led to gentle folding and dip angles of $\sim 15^\circ$. Continued folding caused tightening of folds, accommodated by slip on bedding-parallel faults at progressively steeper dip. The tightness of folds is then limited by the weakness of bedding planes, which determined the steepest angle at which fault slip was possible. This appears to be $< 75^\circ$ for most faults (Fig. 4), as expected from Andersonian mechanics with clay-rich fault planes, but a few steeper exceptions exist. Craddock et al. (2007) suggested that folding was followed by transport on discrete thrust faults with a top-to-the north shear sense. This is possible, and may have occurred as folds tightened to a point where slip on larger discrete faults, not observed in the field area but possibly present at the contacts between formations (e.g. Lindeque et al., 2011), became preferable. It is also possible that the folding in the Prince Albert Formation accommodates a relatively small component of shortening, compared to displacements on gently dipping thrusts that are not exposed, but have been inferred on geophysical profiles (Stankiewicz et al., 2007; Lindeque et al., 2011).

Folding clearly dominates the deformation within the Prince Albert Formation, but appears largely accommodated by localized bedding-parallel slip, with subsidiary bedding-discordant faults. Bedding-discordant faults have a similar frequency-distribution of dip angles as bedding-parallel faults, with prevalence of dip angles in the range 30° to 60°, but with some faults dipping at more than 80°. Some of the very steep faults are in fold hinges (e.g. Fig. 2a), and appear to have initiated as bedding-parallel, and cross-cut bedding where the dip angle is gentle near the fold hinge. Other steep faults are at relatively low (30° or less) angles to bedding, and may represent faults that occurred before folding, and were then rotated into their current orientation during folding. This interpretation, and the observation that there is little soft sediment deformation in the Prince Albert Formation, is important because it seems likely that the Prince Albert Formation was lithified and comprising rigid beds separated by weak bedding planes before north-south shortening occurred. This supports the suggestion of Tankard et al. (2009) that deformation in the Cape Fold Belt initiated in the Triassic (rather than the Permian or Carboniferous), after burial and diagenesis of Permian sediments.

6.2. *Fault Spacing*

Distances between adjacent bedding-parallel shear veins are variable (0.1 - 7 m) and heterogeneous (Fig. 5). Typically, shear surfaces in flexural slip folds are closer together in steeper dipping fold limbs to accommodate greater flexural slip, whereas in gently dipping fold limbs the relative amount of flexural slip is less and therefore shear surfaces are spaced further apart (Horne and Culshaw, 2001; Hayes and Hanks, 2008). However, the studied folds are relatively upright and do not vary greatly in interlimb angle, so that variation in limb dip is unlikely to be a major factor explaining the variation in slickenfiber vein spacing.

Although the shear veins accommodating flexural slip are along bedding planes, they are spaced further apart than the typical bedding thickness of ~ 0.3 m in the Prince Albert Formation. Fowler and Winsor (1997) argue that the formation of bedding-parallel shear veins occurs at interfaces between relatively competent and incompetent sedimentary layers during progressive folding, driven by a gradient in shear strain rate at such interfaces. This effect may have played a role in developing shear veins at the interface between massive (clay-poor) and cleaved (clay-rich) layers in the Prince Albert Formation; however, there are closely spaced shear veins also between clay-rich layers (e.g. Fig. 2a), where this explanation is not sufficient.

Opening vein-filled fractures, particularly fractures filled by subhedral to euhedral quartz that indicates growth into a fluid filled crack (such as in Fig. 7c), requires elevated fluid pressure (Oliver and Bons, 2001; Bons et al., 2012). High fluid pressure assisting vein opening and growth may have been accentuated by the presence of relatively impermeable bedding layers within the Prince Albert Formation that could behave as seals (e.g. Sibson, 1990; Cox et al., 2001). This could result in localized areas of high fluid pressure and associated formation of bedding-parallel veins. Fold hinge zones are generally zones toward which material migrate during fluid-assisted deformation by pressure solution (Ramsay, 1977), and it is clear in Fig. 2a that the density of slickenfiber-coated bedding-parallel veins, at least locally, increases in the fold hinge region. This may relate to decreased slip and increased bedding-perpendicular dilation in the hinge region, such that bedding-parallel veins become dominantly tensile. More tensile opening would require thicker veins or a greater density of veins. This is consistent with slickenfiber-coated bedding-parallel veins forming during flexural slip, because bedding-parallel displacement along fold limbs would need to be accompanied by bedding-normal displacement at the fold hinge, as testified by thickened veins and reversal in shear sense across hinge regions.

Although bedding-layer competency contrast is also likely to have an effect, fluid pressure variations may have been the primary control on the spacing of bedding-parallel veins in the Prince Albert Formation. This interpretation may be biased by the relatively easy preservation of bedding-parallel slickenfiber veins compared to any bedding-parallel slip surfaces along which no vein developed. It could be that the observed spacing of bedding-parallel slickenfiber veins differs from the actual spacing of shear surfaces during folding. An alternative to a fluid pressure controlled fault spacing is therefore that the fault spacing was controlled by competency contrasts (Fowler and Winsor, 1997), but as veins formed preferentially along high fluid pressure faults, slip surfaces from high fluid pressure zones have been preferentially preserved.

6.3. Stress and Fluid Pressure Conditions During Flexural Slip

Where developed, tensile fractures in the Cape Fold Belt, and in the Prince Albert Formation, are commonly subhorizontal (Craddock et al., 2007), as expected for an Andersonian stress regime favoring reverse faulting. An exeption, however, is bedding-normal veins developed in some fold hinges, where these veins accommodate local tensile stresses caused by bending of relatively rigid beds. In addition, inclusion bands developed within flexural slip shear veins are generally at 50° to 70° to vein margins dipping at 50° to 70°, i.e. also roughly horizontal. These inclusion bands are developed by consecutive cracking and sealing (Ramsay, 1980; Cox and Etheridge, 1983; Renard et al., 2005; Fagereng et al., 2010), and likely reflect the orientation of tensile fractures in a micro-dilational jog (Fig. 6a). Subvertical, pressure solution cleavage also supports a regime where σ_1 is horizontal, and σ_3 is vertical. For the following discussion, the assumption is therefore made that during flexural slip folding, σ_1 was horizontal, and perpendicular to cleavage, i.e. north trending, and σ_3 was vertical. We apply traditional Mohr-Coulomb mechanics and consider conditions of slip nucleation on existing weak surfaces within otherwise intact rock.

As discussed above, slickenfiber veins represent incremental slip on surfaces ranging from well to poorly oriented, implying that reshear occurred on progressively more unfavourably oriented surfaces as folding progressed. Ideally oriented faults would be dipping at 30° to 37° in these quartz-clay rocks, and lack of optimally oriented discordant faults (Fig. 4) implies that frictional failure of surrounding rock, initiating new faults, was not a preferred brittle deformation mode during folding. However, tensile failure of rock immediately surrounding slip surfaces must have occurred to create macroscopic, layered, slickenfibers containing wall rock fragments. One mechanism to grow such fibers was suggested by Fagereng et al. (2010)

and termed 'dilational hydroshear'. In this mechanism, shear failure along weak planes occurs coincidentally with tensile failure of surrounding rock, such that conditions must prevail where a shear failure criterion is reached along a pre-existing surface at the same time as the hydrofracture criterion is achieved in the host rock of this shear surface. This implies the fluid pressure, P_f, must equal σ_3 plus the tensile strength of the host rock, T_0, and that differential stress is less than $4T_0$ (Secor, 1965; Etheridge, 1983). For frictional reactivation to occur at the same time as tensile failure, the following criterion must be met (Sibson, 2009; Fagereng et al., 2010):

$$(\sigma_1 - \sigma_3) = \frac{\tan\theta_r + \cot\theta_r}{1 - \mu_s \tan\theta_r} \times (c - \mu_s T_0) \tag{1}$$

where c is the cohesion of the slip surface. For shear surfaces with low cohesion (0.1 MPa) and assuming a tensile strength of 1 to 10 MPa for surrounding mudstone (Lockner, 1995), conditions for 'dilational hydroshear' as a function of reactivation angle θ_r are estimated in Fig. 9. This mechanism of concurrent slip and tensile fracture appears to only occur on unfavorable to severely misoriented faults, as a positive $(\sigma_1 - \sigma_3)$ value is only obtained for θ_r in excess of about 60° for μ_s of 0.6, and over 75° for μ_s of 0.3. It may therefore be that flexural slip occurred along bedding planes from an early stage of folding, but only produced slickenfiber-coated fault surfaces involving coincident shear and dilation as progressive folding led to steepening of fold limbs and slip occurred on weak, unfavorably oriented planes. If this interpretation is correct, then at least some slickenfibers reflect slip allowed by high fluid pressure at unfavorable conditions for reactivation. In this case, that would mean than flexural slip folding in the Prince Albert Formation mudstones continued, at least locally, after faults steepened to unfavorable angles, and that this was allowed by fluid pressures in excess of lithostatic along weak bedding planes. Slickenfibre laminae with quartz morphology not involving crack-seal bands at high angles to slip surfaces, may have formed by frictional reactivation of more preferably oriented planes, but it is then intriguing that crack-seal bands were not preserved. This lack of crack-seal band preservation may indicate a difference in fault slip style between well and poorly oriented planes, potentially governed by the maximum contained overpressure.

An alternative mechanism for slickenfiber growth involves slip assisted by dissolution-precipitation creep, a viable mechanism in fine grained rocks with a pressure solution cleavage (Bos et al., 2000; Bos and Spiers, 2001; Niemeijer and Spiers, 2006; Gratier and Gueydan, 2007; den Hartog and Spiers, 2014). In this model, pressure solution allows for dissolution of asperities (irregularities) along the slip surface, and precipitation occurs in low-stress dilatant sites, without necessarily requiring brittle fracture (Gratier and Gueydan, 2007). This is a possible mechanism in the temperature window of 150 - 200°C that is proposed for the Cape Fold Belt, as fine grain sizes and mobility of silica in solution at these conditions are favorable for pressure solution (Fagereng, 2014). However, the highly localized slip required for flexural slip rather than flexural flow, velocity-weakening behavior observed in quartz in this temperature range (Blanpied et al., 1995), and the presence of cataclasites along slip surfaces, indicate that at least a component of frictional sliding is likely for the flexural slip folds in the Prince Albert Formation.

6.4. Fault Slip Style

Vein quartz in shear veins from the Prince Albert Formation is largely unaffected by post-precipitation deformation and recrystallization, an effect of the low temperature of precipitation (well below the onset of quartz plasticity at $\sim 350°$C, Hirth et al., 2001). We therefore use the microstructure of these veins to discuss the kinematics and mechanics of flexural slip that accommodated deformation during the folding in the Prince Albert Formation.

In places, the shear veins preserve a crack-seal microstructure. The crack-seal bands have a relatively consistent spacing (within an order of magnitude) along single shear surfaces, but spacing varies by orders of magnitude between transects from different veins (Fig. 8). The spacing between inclusion bands reflects the sealed crack from each individual crack-seal episode (Ramsay, 1980; Cox and Etheridge, 1983; Cox, 1987). This spacing is therefore a minimum estimate for the crack aperture, as the crack may not have been completely sealed. It is possible for a crack-seal structure to form by continuous fault slip, if continuous vein opening is coupled to a precipitation rate that increases with time until the crack is filled, and then a new crack forms adjacent to the sealed crack (Lee and Wiltschko, 2000). This mechanism would, however, require that vein growth rate can increase during sealing of each growth increment. In the veins studied here, crystals are usually continuous across inclusion bands, implying that the size and orientation of crystal faces stay approximately constant, and unless other parameters change significantly growth rate should not increase during sealing. Alternatively, the presence of inclusion bands implies incremental slickenfiber growth (e.g. Renard et al., 2005; Fagereng et al., 2011). In this case, vein opening is faster than precipitation, and sealing occurs at a constant or decreasing rate (e.g. Lee and Wiltschko, 2000). The blocky and elongate-blocky quartz morphology that is predominant in the Prince Albert Formation veins is generally inferred to be associated with growth into open cracks

(Cox, 1987; Oliver and Bons, 2001; Bons et al., 2012), rather than slow subcritical grain growth which is more commonly associated with fibrous growth (Urai et al., 1991; Fisher and Brantley, 1992). Therefore, we infer that the crack-seal bands developed along faults accommodating flexural slip in the Prince Albert Formation reflect incremental slip where each slip episode created a dilatant crack which was subsequently filled by quartz precipitation.

A number of interpretations can be made based on the inference that crack-seal bands reflect episodic fault slip. Another inference we have made, is that the slickenfiber veins containing crack-seal bands, reflecting tensile cracks, formed on faults active at fluid pressures locally in excess of σ_3. Each crack event is then associated with a point in time where fluid pressure was locally lithostatic, because σ_3 is inferred as vertical, and sealing reflects precipitation of quartz driven by the fluid pressure drop induced by crack dilation. In this case, slip along bedding planes occurs as fluid pressure reaches a critical value, and is relatively independent of fluctuations in shear stress. Consequently, the relatively consistent inclusion band spacing along any transect implies cycling of fluid pressure levels and failure at a relatively constant maximum contained fluid pressure. These two interpretations, that slip on slickenfiber-coated bedding surfaces was controlled by fluid pressure fluctuations, and led to creation of open space in characteristic increments, lead to a third inference; flexural slip involved stick-slip motion along unfavourably oriented bedding planes, at least in late stages of folding.

Stick-slip motion is generally associated with earthquake slip, and incrementally grown slickenfibers with crack-seal bands at a high angle to vein walls may therefore reflect episodic earthquake slip on unfavorably oriented faults under low effective stress conditions. Slip increments on the order of 10 μm to 1000 μm on faults that are continuous for tens to hundreds of meters, imply a ratio of average slip, $\bar{u}$, to potential rupture length, L, of $10^{-6} < \bar{u}/L < 10^{-5}$. Because fault length likely increases as a fault grows by incremental slip, this is likely an underestimate of $\bar{u}/L$, as each slip event likely had a smaller L than the entire available fault length. Stress drop, $\Delta\tau$, is related to $\bar{u}/L$ with the relation $\Delta\tau = CG\bar{u}/L$ (Kanamori and Anderson, 1975), where C is a geometrical factor, and G is the shear modulus and typically 30 GPa in the brittle crust (Turcotte and Schubert, 2002). For a circular rupture where $C = 7\pi/16$, the stress drop for slip increments in this study can then be estimated as roughly between 40 and 400 kPa, although locally higher and lower stress drops could have occurred. Although significant uncertainties are involved in these numbers, episodic slip events recorded in crack-seal slickenfiber veins here appear to have stress drops of no more than a few hundred kPa, on the low end of the range of stress drops calculated for geophysically observed events (Scholz, 2002). The magnitudes of such events would be small; an average slip of 30 μm on a 10 m radius (r) fault would give a moment, defined as $M_0 = G\pi r^2 \bar{u}$ for a circular rupture (Aki, 1967), of approximately 3×10^8 Nm. Larger slip of 1 mm over a 100 m radius fault would give a moment of about 9×10^{11} Nm. Taking moment magnitude, M_w, as equal to $2/3(\log M_0 - 9.1)$ (Purcaru and Berckenhemer, 1978; Hanks and Kanamori, 1979), this moment range translates to a moment magnitude range of -0.5 to +1.9. Repeating low stress drop events in this small magnitude range is comparable to observations of low frequency earthquakes in subduction zones (Ito and Obara, 2006; Peng and Gomberg, 2010) and repeating microseismicity on the San Andreas fault (Nadeau et al., 1995; Nadeau and McEvilly, 2004). A mechanism analogous to repeating small, possibly low stress drop, earthquakes, was also suggested for the formation of slickenfiber veins in an exhumed accretionary mélange by Fagereng et al. (2011).

As opposed to slickenfiber veins studied by Fagereng et al. (2011), the slickenfibers involved in flexural slip folding in this study do not have a uniform crack-seal structure, but also include significant segments and layers defined by a blocky microstructure. Blocky quartz, as well as subhedral and elongate-blocky crystals present in places, imply growth into an open space that opened in one event. Also, for these microstructures to be preserved, rather than fibrous quartz, vein opening rate likely exceeded growth rate (Lee and Wiltschko, 2000; Bons et al., 2012). Accordingly, the slickenfiber veins do not exclusively record episodic crack-seal growth representing tens to hundreds of events (as depicted in Fig. 8), but also single slip events of greater magnitude. There is also a possibility that some of these events occurred by a 'crack-seal, slip' mechanism as proposed by Petit et al. (1999). This would imply that slip along shear surfaces, preserved as cataclasites, led to dilatant opening of zones between slip surfaces (as in Fig. 6a), and these areas were then sealed over time, until a new slip event may have occurred. There is no constraint on reactivation angle relative to σ_3 in slickenfiber veins that lack crack-seal bands reflecting tensile opening in cracks at a high angle to slip surfaces. It is possible, therefore, that slickenfibers formed by this 'crack-seal. slip' mechanism reflect shear under lower contained fluid pressure, at optimal or less unfavourable orientation than the slip by the dilational shear mechanism outlined above.

Overall, the slickenfiber veins reflect a variety of slip increment magnitudes, associated with dilatancy allowing for quartz precipitation. In places, incremental stick-slip is evident from blocky quartz microstructures and crack-seal inclusion bands, reflecting tens to hundreds of slip increments of characteristic order of magnitude, and possibly reflecting repeating micro-earthquakes. We infer these microstructures to have formed under high fluid pressures to explain the high angle between coincident shear end tensile fracture. In other places, larger zones of blocky, elongate-blocky, and euhedral to subhedral quartz, adjacent to cataclastic slip surfaces, indicate larger and possibly single event slip increments. This latter slip style may reflect shear under lower fluid pressure conditions along well-oriented to slightly misoriented planes. This variety in slickenfiber microstructures may indicate that multiple fault slip styles occurred on a single fault segment, potentially as a function of increasingly unfavorable orientation as faults steepened with progressive folding.

7. Conclusions

In conclusion, we have made a number of observations and inferences regarding slickenfiber veins associated with flexural slip folding in the Prince Albert Formation of the Karoo foreland basin of the Cape Fold Belt. We suggest that these veins formed by localised frictional sliding within a zone of distributed deformation. The veins therefore reflect fault slip styles recorded from a zone of mixed continuous-discontinuous deformation.

1. Bedding-parallel slickenfiber veins thicken in fold hinges and show a reversal in shear-sense such that the hanging wall moves toward the hinge line on both sides of the hinge. As a result, there is no shear displacement at the hinge, but rather a component of bedding-perpendicular extension. The veins commonly also cross-cut axial planar cleavage. Bedding-parallel slickenfiber veins are therefore inferred to have formed progressively during flexural slip folding.
2. Bedding planes that accommodated flexural slip during folding are characterized by slickenfibre-coated surfaces, and typically dip at angles greater than the optimal reactivation angle of 30° to 37°. The range in dip angles indicates faults ranging in orientation from well to poorly oriented, as expected if folds tighten progressively until lock-up angles are reached.
3. Slickenfiber veins formed by a mixture of slip styles, but generally involving stick-slip behavior along one or more shear surfaces. Some veins record tens to hundreds of slip increments on the order of tens of micrometers to a few millimeters, whereas other veins reflect quartz precipitation into open spaces that imply slip increments of as much as a few centimeters.
4. Shear veins locally contain subhorizontal crack-seal bands and are in places associated with subhorizontal tensile fractures. Formation of these tensile fractures imply fluid

pressures in excess of the least compressive stress, which was subvertical and therefore approximately lithostatic. Flexural slip folding in this location therefore, locally and likely in late stages of folding, involved slip on low cohesion, weak planes, assisted by local and transient lithostatic fluid pressure conditions.

5. Stick-slip deformation along bedding-planes, occurring under low effective stress conditions, may reflect low stress drop seismic events as recorded in some subduction zones and along the San Andreas fault. The mixture of slip increments and vein quartz microstructures within any one slickenfiber vein highlights the possibility that a single fault can be capable of several fault slip styles, including slow, fast, and intermediate slip rates. The type of fault slip may be governed by the local maximum contained overpressure, which is again governed by the degree of misorientation of planes available for reactivation. Increasing misorientation as folds progressively tighten, may therefore lead to slip at decreasing effective stress in late phases of folding as faults begin to lock up. Active flexural slip folding may therefore be associated with a complex deformation pattern involving continuous deformation of folded layers accompanied by variable magnitude frictional stick-slip along discrete, mostly bedding-parallel, fault surfaces, at least until slip on new, through-going fault surfaces becomes preferable.

Acknowledgments

This work was supported by an NRF incentive grant for rated researchers to Å.F. We greatly appreciate reviewer comments from Francesca Remitti and John Cosgrove, which significantly improved the manuscript.

References

Aki, K., 1967. Scaling law of seismic spectrum. Bulletin of the Seismological Society of America 72, 1217–1231.

Bangert, B., Stollhofen, H., Lorenz, V., Armstrong, R., 1999. The Geochronology and significance of ash-fall tuffs in the glaciogenic Carboniferous-Permian Dwyka Group of Namibia and South Africa. Journal of African Earth Sciences 29, 33–49.

Blanpied, M. L., Lockner, D. A., Byerlee, J. D., 1995. Frictional slip of granite at hydrothermal conditions. Journal of Geophysical Research 100, 13,045–13,064.

Bons, P. D., Elburg, M. A., Gomez-Rivas, E., 2012. A review of the formation of tectonic veins and their microstructures. Journal of Structural Geology 43, 33–62.

Bos, B., Peach, C. J., Spiers, C. J., 2000. Frictional-viscous flow of simulated fault gouge caused by the combined effects of phyllosilicates and pressure solution. Tectonophysics 327, 173–194.

Bos, B., Spiers, C., 2001. Experimental investigation into the microstructural and mechanical evolution of phyllosilicate-bearing fault rock under conditions favouring pressure solution. Journal of Structural Geology 23, 1187–1202.

Byerlee, J. D., 1978. Friction of rocks. Pure and Applied Geophysics 116, 615–626.

Catuneanu, O., Hancox, P. J., Rubidge, B. S., 1998. Reciprocal flexural behaviour and contrasting stratigraphies: a new basin development model for the Karoo foreland system, South Africa. Basin Research 10, 417–439.

Catuneanu, O., Wopfner, H., Eriksson, P. G., Cairncross, B., Rubidge, B. S., Smith, R. M. H., Hancox, P. J., 2005. The Karoo basins of south-central Africa. Journal of African Earth Sciences 43, 211–253.

Chapple, W. M., Spang, J. H., 1974. Significance of layer-parallel slip during folding of layered sedimentary rocks. Geologcal Society of America Bulletin 85, 1523–1534.

Collettini, C., De Paola, N., Goulty, N. R., 2006. Switches in the minimum compressive stress direction induced by overpressure beneath a low-permeability fault zone. Terra Nova 18, doi:10.1111/j.1365–3121.2006.00683.x.

Cosgrove, J. W., 1993. The interplay between fluids, folds and thrusts during the deformation of a sedimentary succession. Journal of Structural Geology 15, 491–500.

Cox, S. F., 1987. Antitaxial crack-seal vein microstructures and their relationships to displacement paths. Journal of Structural Geology 9, 779–788.

Cox, S. F., Etheridge, M. A., 1983. Crack-seal fibre growth mechanisms and their significance in the development of oriented layer silicate microstructures. Tectonophysics 92, 147–170.

Cox, S. F., Knackstedt, M. A., Braun, J., 2001. Principles of structural control on permeability and fluid flow in hydrothermal systems. In: Richards, J., Tosdal, R. (Eds.), Deformation, Fluid Flow and Ore Deposits. Vol. 14 of Reviews in Economic Geology. pp. 1–24.

Craddock, J. P., McKiernan, A. W., de Wit, M. J., 2007. Calcite twin analysis in syntectonic calcite, Cape Fold Belt, South Africa: Implications for fold and cleavage formation within a shallow thrust front. Journal of Structural Geology 29, 1100–1113.

de Swart, A. M. J., Rowsell, D. M., 1974. Note on the relationship between diagenesis and deformation in the Cape Fold Belt. Transactions of the Geological Society of South Africa 77, 239–245.

de Wit, M. J., Ransome, I. G. D., 1992. Regional inversion tectonics along the southern margin of Gondwana. In: de Wit, M. J., Ransome, I. G. D. (Eds.), Inversion Tectonics of the Cape Fold Belt, Karoo, and Cretaceous Basins of Southern Africa. Balkema, Amsterdam, pp. 15–22.

den Hartog, S. A. M., Spiers, C. J., 2014. A microphysical model for fault gouge friction applied to subduction megathrusts. Journal of Geophysical Research 119, 1510–1529.

du Toit, A. L., 1937. Our Wandering Continents. Oliver and Boyd, Edinburgh.

Durney, D. W., Ramsay, J. G., 1973. Incremental strains measured by syntectonic crystal growths. In: De Jong, K., Scholten, R. (Eds.), Gravity and Tectonics. Wiley, New York, pp. 67–96.

Etheridge, M. A., 1983. Differential stress magnitudes during regional deformation and metamorphism - upper bound imposed by tensile fracturing. Geology 11, 231–234.

Fagereng, A., 2012. A note on folding mechanisms in the Cape Fold Belt, South Africa. South African Journal of Geology 115, 137–144.

Fagereng, A., 2014. Significant shortening by pressure solution creep in Dwyka diamictite, Cape Fold Belt, South Africa. Journal of African Earth Sciences 97, 9–18.

Fagereng, A., Remitti, F., Sibson, R. H., 2010. Shear veins observed within anisotropic fabric at high angles to the maximum compressive stress. Nature Geoscience 3, 482–485, doi:10.1038/NGEO898.

Fagereng, A., Remitti, F., Sibson, R. H., 2011. Incrementally developed slickenfibers - geological record of repeating low stress-drop seismic events? Tectonophysics 510, 381–386.

Fagereng, A., Smith, Z., Rowe, C. D., Makhubu, B., Sylvester, F. Y. G., 2014. Stress, strain and fault behavior at a thrust ramp: Insights from the Naukluft thrust, Namibia. Journal of Structural Geology 58, 95–107.

Fisher, D., Brantley, S. L., 1992. Models of quartz overgrowth and vein formation: deformation and fluid flow in an ancient subduction zone. Journal of Geophysical Research 97, 20.043–20.061.

Fitches, W. R., Cave, R., Craig, J., Maltman, A. J., 1986. Early veins as evidence of detachment in the Lower Palaeozoic rocks of the Welsh Basin. Journal of Structural Geology 8, 607–620.

Fowler, T. J., 1996. Flexural-slip generated bedding-parallel veins from central Victoria, Australia. Journal of Structural Geology 18, 1399–1415.

Fowler, T. J., Winsor, C. N., 1997. Characteristics and occurrence of bedding-parallel slip surfaces and laminated veins in chevron folds from the Bendigo- Castlemaine goldfields: implications for flexural-slip folding. Journal of Structural Geology 19, 799–815.

Frimmel, H. E., Fölling, P. G., Diamond, R., 2001. Metamorphism of the Permo-Triassic Cape Fold Belt and its basement, South Africa. Mineralogy and Petrology 73, 325–346.

Gratier, J. P., Gueydan, F., 2007. Deformation in the presence of fluids and mineral reactions. In: Handy, M. R., Hirth, G., Hovius, N. (Eds.), Tectonic Faults: Agents of Change on a Dynamic Earth. MIT Press, pp. 319–356.

Hälbich, I. W., 1992. The Cape Fold Belt oorogen: State of the art 1970s-1980s. In: de Wit, M. J., Ransome, I. G. D. (Eds.), Inversion Tectonics of the Cape Fold Belt, Karoo, and Cretaceous Basins of Southern Africa. Balkema, Amsterdam, pp. 141–158.

Hanks, T. C., Kanamori, H., 1979. A moment magnitude scale. Journal of Geophysical Research 84, 2348–2350.

Hayes, M., Hanks, C. L., 2008. Evolving mechanical stratigraphy during detachment folding. Journal of Structural Geology 30, 548–564.

Hirth, G., Teyssier, C., Dunlap, W., 2001. An evaluation of quartzite flow laws based on comparisons between experimentally and naturally deformed rocks. International Journal of Earth Sciences 90, 77–87.

Horne, R., Culshaw, N., 2001. Flexural-slip folding in the Meguma Group, Nova Scotia, Canada. Journal of Structural Geology 23, 1631–1652.

Ito, Y., Obara, K., 2006. Very low frequency earthquakes within accretionary prism are very low stress-drop earthquakes. Geophysical Research Letters 33, doi:10.1029/2006GL025883.

Johnson, M. R., van Vuuren, C. J., Hegenberger, W. F., Key, R., Shoko, U., 1996. Stratigraphy of the Karoo Supergroup in southern Africa: an overview. Journal of African Earth Sciences 23, 3–15.

Johnson, M. R., van Vuuren, C. J., Visser, J. N. J., Cole, D. I., Wickens, H. d., Christie, A. D. M., Roberts, D. L., Brandl, G., 2006. Sedimentary rocks of the Karoo Supergroup. In: Johnson, M. R., Anhaeusser, C. R., Thomas, R. J. (Eds.), The Geology of South Africa. The Geological Society of South Africa, Johannesburg/Council for Geoscience, Pretoria, pp. 461–499.

Kanamori, H., Anderson, D. L., 1975. Theoretical basis of some empirical relations in seismology. Bulletin of the Seismological Society of America 65, 1073–1095.

Koehn, D., Passchier, C. W., 2000. Shear sense indicators in striped bedding-veins. Journal of Structural Geology 22, 1141–1151.

Lee, Y. J., Wiltschko, D., 2000. Fault controlled sequential vein dilation: competition between slip and precipitation rates in the Austin Chalk, Texas. Journal of Structural Geology 22, 1247–1260.

Lindeque, A., de Wit, M. J., Ryberg, T., Weber, M., Chevallier, L., 2011. Deep crustal profile across the southern Karoo Basin and Beattie Magnetic Anomaly, South Africa: An integrated interpretation with tectonic implications. South African Journal of Geology 114, 265–292.

Lock, B. E., 1980. Flat-plate subduction and the Cape Fold Belt of South Africa. Geology 8, 35–39.

Lockner, D. A., 1995. Rock failure. In: Rock Physics and Phase Relations, A Handbook of Physical Constants. American Geophysical Union, Washington D.C., pp. 127–147.

Mittempergher, S., Pennacchioni, G., Di Toro, G., 2009. The effects of fault orientation and fluid infiltration on fault rock assemblages at seismogenic depths. Journal of Structural Geology 31, 1511–1524.

Morrow, C., Radney, B., Byerlee, J., 1992. Frictional strength and the effective pressure law of montmorillonite and illite clays. In: Evans, B., Wong, T. (Eds.), Fault Mechanics and Transport Properties of Rocks. Academic Press, London, pp. 69–88.

Nadeau, R. M., Foxall, R. M., McEvilly, T. V., 1995. Clustering and periodic recurrence of microearthquakes on the San Andreas Fault at Parkfield, California. Science 267, 503–507.

Nadeau, R. M., McEvilly, T. V., 2004. Periodic pulsing of characteristic microearthquakes on the San Andreas fault. Science 303, 220–222.

Nicholson, R., 1978. Folding and pressure solution in a laminated calcite-quartz vein from the Silurian slates of the Llangollen region of N Wales. Geological Magazine 115, 47–54.

Niemeijer, A., Spiers, C., 2006. Velocity dependence of strength and healing behaviour in phyllosilicate-bearing fault gouge. Tectonophysics 427, 231–253.

Oliver, N. H., Bons, P. D., 2001. Mechanisms of fluid flow and fluid-rock interaction in fossil metamorphic hydrothermal systems inferred from vein-wallrock patterns, geometry and microstructure. Geofluids 1, 137–162.

Peng, Z., Gomberg, J., 2010. An integrated perspective of the continuum between earthquakes and slow slip phenomena. Nature Geoscience 3, 599–607.

Petit, J. P., Wibberley, C. A. J., Ruiz, G., 1999. 'crack-seal', slip: a new fault valve mechanism? Journal of Structural Geology 21, 1199–1207.

Purcaru, G., Berckenhemer, H., 1978. A magnitude scale for very large earthquakes. Tectonophysics 49, 189–198.

Ramsay, J. G., 1975. Development of chevron folds. Geological Society of America Bulletin 85, 1741–1754.

Ramsay, J. G., 1977. Pressure solution - the field data. Journal of the Geological Society 134, 72.

Ramsay, J. G., 1980. The crack-seal mechanism of rock deformation. Nature 284, 135–139.

Ramsay, J. G., Huber, M. I., 1983. The Techniques of Modern Structural Geology. Volume 1: Strain Analysis. Academic Press, London.

Ramsay, J. G., Huber, M. I., 1987. The Techniques of Modern Structural Geology. Volume 2: Folds and Fractures. Academic Press, London.

Renard, F., Andréani, M., Boullier, A.-M., Labaume, P., 2005. Crack-seal patterns: records of uncorrelated stress release variations in crustal rocks. In: Gapais, D., Brun, J. P., Cobbold, P. R. (Eds.), Deformation Mechanics, Rheology and Tectonics: from Minerals to the Lithosphere. Vol. 243 of Geological Society of London Special Publication. Geological Society of London, pp. 67–79.

Scholz, C. H., 1988. The brittle-plastic transition and the depth of seismic faulting. Geologische Rundschau 77, 319–328.

Scholz, C. H., 2002. The Mechanics of Earthquakes and Faulting, 2nd Edition. Cambridge University Press.

Secor, D. T., 1965. Role of fluid pressure in jointing. American Journal of Science 263, 633–646.

Sibson, R. H., 1984. Roughness at the base of the seismogenic zone: Contributing factors. Journal of Geophysical Research 89, 5791–5799.

Sibson, R. H., 1985. A note on fault reactivation. Journal of Structural Geology 7, 751–754.

Sibson, R. H., 1990. Rupture nucleation on unfavourably oriented faults. Bulletin of the Seismological Society of America 80, 1580–1604.

Sibson, R. H., 2009. Rupturing in overpressured crust during compressional inversion-the case from NE Honshu, Japan. Tectonophysics 473, 404–416, doi:10.1016/j.tecto.2009.03.016.

Stankiewicz, J., Ryberg, T., Schulze, A., Lindeque, A., Weber, M. H., de Wit, M. J., 2007. Initial results from wide-angle seismic refraction lines in the southern Cape. South African Journal of Geology 110, 407–418.

Tankard, A., Welsink, H., Aukes, P., Newton, R., Stettler, E., 2009. Tectonic evolution of the Cape and Karoo basins of South Africa. Marine and Petroleum Geology 26, 1379–1412.

Tanner, P. W. G., 1989. The flexural-slip mechanism. Journal of Structural Geology 12, 1084–1087.

Turcotte, D. L., Schubert, G., 2002. Geodynamics, 2nd Edition. Cambridge University Press, Cambridge, UK.

Urai, J. L., Williams, P. F., van Roermund, H. L. M., 1991. Kinematics of crystal growth in syntectonic fibrous veins. Journal of Structural Geology 13, 823–836.

Visser, J. N. J., 1990. The age of the late Palaeozoic glacigene deposits in southern Africa. South African Journal of Geology 93, 366–375.

Visser, J. N. J., 1992. Deposition of the Early to Late Permian Whitehill Formation during a sea-level high stand in a juvenile foreland basin. Transactions of the Geological Society of South Africa 95, 181–193.

Table and Figure Captions

Figure 1: Location of the study area. a) Overview of southern Africa, with the extent of the Main Karoo Basin and the Cape Fold Belt (after Johnson et al., 1996), the rectangle showing the study area related to the map in panel (c). b) Schematic cross-section of the Cape Fold Belt and the Karoo Basin, based on a composite cross-section east of the study area, compiled by Tankard et al. (2009). c) Local geology in the area around Laingsburg, same legend as in (b), after the 1:1,000,000 geological map of South Africa. The dashed rectangle shows the area from which samples and measurements were collected.

Figure 2: Field photographs. a) Small antiform within the Prince Albert Formation, bedding-parallel slickenfiber-coated veins are highlighted in dashed red lines, discordant slickenfiber-coated faults are in yellow. b) Fold hinge zone with massive, fractured, clay-poor bed and cleaved, clay-rich beds, separated by slickenfiber-coated shear veins. Note thickening of bedding-parallel vein in the fold hinge, where the shear displacement is zero as the vein opening vector is bedding-normal rather than bedding-oblique in this location. c) Close-up of slickenfiber coated bedding plane.

Figure 3: Lower hemisphere, equal area, stereoplots showing orientations of (a) poles to bedding bedding (open circles, n = 103), fold hinge lines (black triangles, n = 29), pencil lineation (red open diamonds, n = 35), and cleavage (dashed great circles, n = 45); and (b) bedding-parallel faults (black solid great circles, n = 57), discordant faults (red dashed great circles, n = 20), and slickenfibers (black, filled circles, n = 79).

Figure 4: Histogram showing the frequency distribution of fault dip angles for bedding-parallel (n = 57) and discordant (n = 20) faults, identified by slickenfiber-coated surfaces.

Figure 5: Spacing of bedding-parallel, slickenfiber-coated veins along a north-south transect, where spacing was measured perpendicular to bedding. a) Cumulative spacing against vein number, where veins are numbered sequentially as they intersect the transect line. Note a few large steps in spacing, within an otherwise near-linear relationship. b) Histogram showing the frequency distribution of vein spacing (n = 65), note a positively skewed distribution with most spacings less than 1 m, but a few instances of several meters spacing between adjacent fault veins.

Figure 6: Geometry of slickenfiber veins. a) Typical model for the development of slickenfiber vein geometry by incremental dilation on an uneven fault surface (after Fagereng et al., 2010; Bons et al., 2012). At time = 0 the fault initiates, and at each increment of slip, dilatant zones open by an amount dependent on the slip magnitude. After n increments of slip (at time = n), a macroscopic slickenfiber with n crack-seal bands has opened. Note that whether crack-seal bands are preserved depends on the relative rates of vein opening and mineral precipitation (Lee and Wiltschko, 2000). In the final vein, fibers may be laminated, with laminae separated by slip surfaces, and containing crack-seal bands (dashed lines in sketch). b) Scanned thin section cut parallel to slickenfibers and perpendicular to the slickenfiber-coated bedding plane. Like the model in (a), this vein comprises multiple quartz laminae separated by slip surfaces (dashed red lines). Note relatively high angle (60 - 70°) between inclusion bands, extension veins (that are parallel to inclusion bands and shown in blue dashed lines), and slip surfaces.

Figure 7: Photomicrographs illustrating the internal geometry and morphology of slickenfiber-coated, bedding-parallel veins from flexural slip folds in the Prince Albert Formation. (a) and (b) are in plane-polarized light, the rest in cross-polarized light. a) Numerous subparallel slip surfaces, defined by wallrock fragments and/or thin cataclasites, lie at approximately 60° to inclusion bands, and separate multiple layers of vein quartz. b) Closer-up view of slip surface and inclusion bands, in a vein that cross-cuts wall rock foliation, which is near-perpendicular to inclusion bands. c) Elongate-blocky quartz within a slickenfiber vein, surrounding a zone of multiple cataclasite slip surfaces. d) Layers of block quartz and calcite separated by slip surfaces that are defined by multiple cataclasites separated by thin damage zones. e) Layers of blocky and euhedral to subhedral quartz separated by a thin slip surface. f) Quartz layer characterised by stretched quartz crystals, with serrated grain boundaries and inclusion bands indicating a crack-seal microstructure.

Figure 8: Locations and data from transects along slip surfaces to measure the spacing between inclusion bands. Left column: sample numbers and thin section scans showing the location of the transects in red lines (circled to be more visible). Middle column: Cumulative spacing of inclusion bands against inclusion band number, where the bands were numbered sequentially as they intersect the transect line. Right column: Histograms illustrating the frequency distribution of inclusion band spacings along each transect.

Figure 9: Conditions for simultaneous frictional reactivation of bedding surfaces with cohesive strength 0.1 MPa, frictional coefficient of μ_s and dip θ_r, and tensile opening of surrounding rock with tensile strength T_0. Calculations using Eq. 1 from Sibson (2009), as adapted by Fagereng et al. (2010). These conditions allow for a mechanism of slickenfiber growth by shear along weak surfaces and concomitant opening of dilational zones between these slip surfaces (as in Fig. 6a), and is only possible for the parameters that yield $(\sigma_1 - \sigma_3) > 1$. For other conditions, shear failure will occur at fluid pressures that are insufficient for concomitant hydrofracturing.

Table 1: Statistics of measured spacing between adjacent inclusion bands along transects shown in Figure 8.

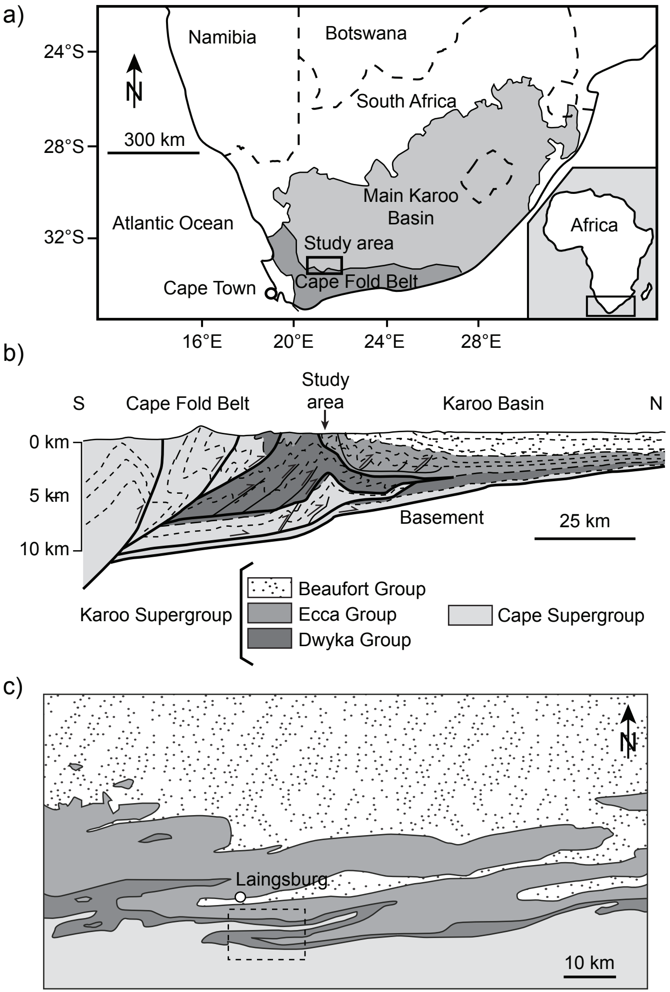
a)
Namibia
Botswana
South Africa
24°S
28°S
32°S
N
300 km
Atlantic Ocean
Main Karoo
Basin
Study area
Cape Fold Belt
Cape Town
Africa
16°E
20°E
24°E
28°E
b)
S
Cape Fold Belt
Study
area
Karoo Basin
N
0 km
5 km
10 km
Basement
25 km
Karoo Supergroup
Beaufort Group
Ecca Group
Dwyka Group
Cape Supergroup
c)
N
Laingsburg
10 km

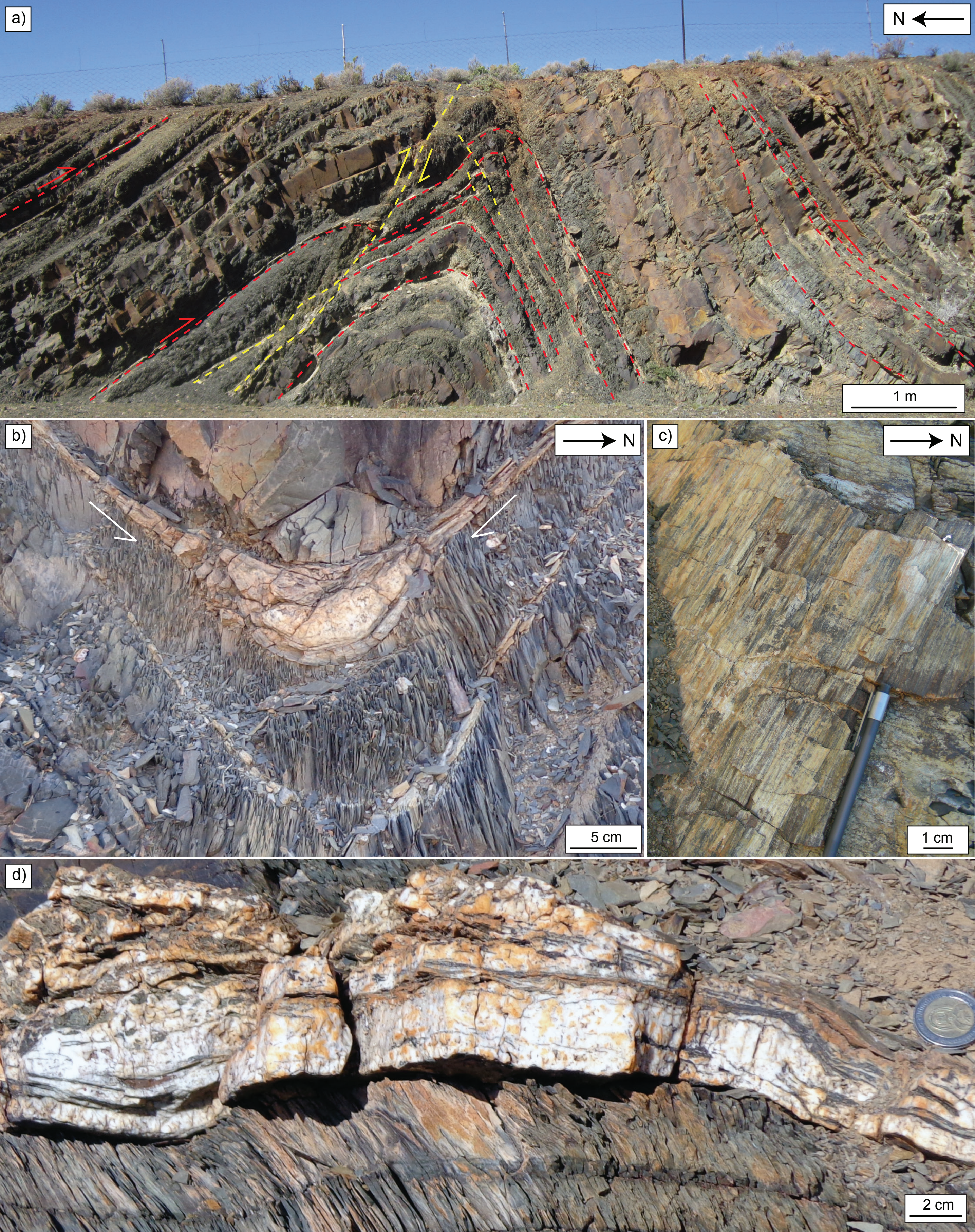
a)
N
1 m
b)
N
5 cm
c)
N
1 cm
d)
2 cm

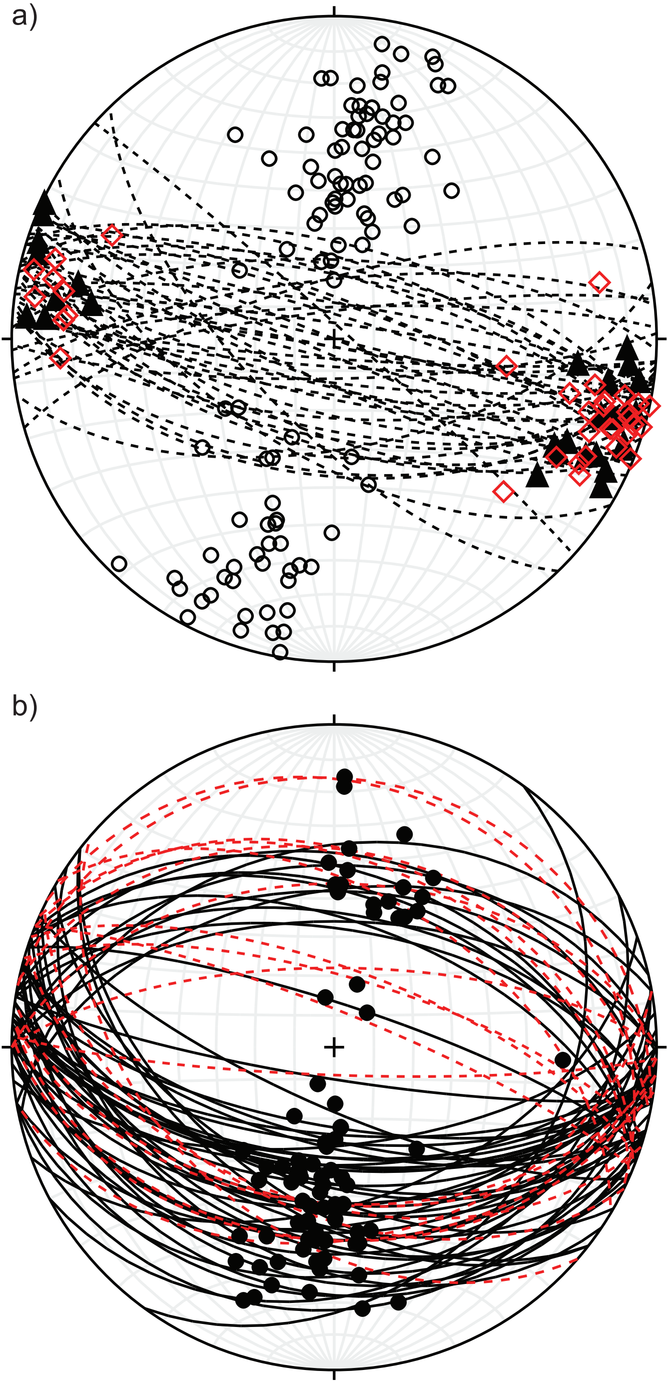
a)
b)

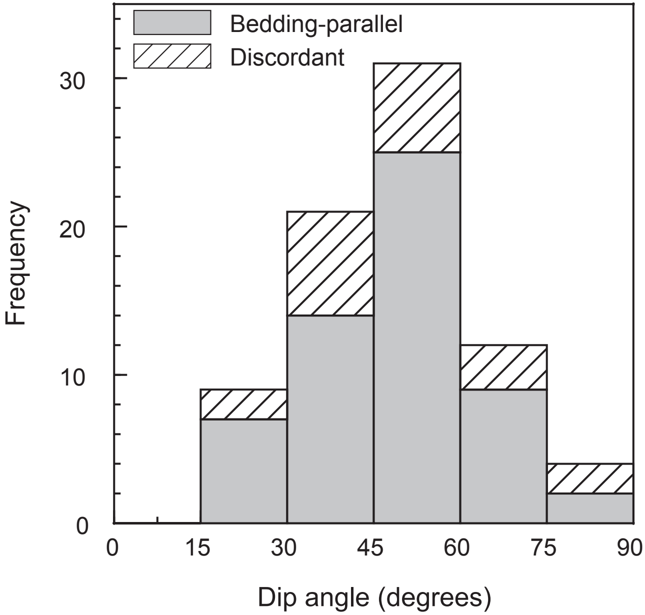
Bedding-parallel
Discordant
Frequency
0
10
20
30
0
15
30
45
60
75
90
Dip angle (degrees)

a)

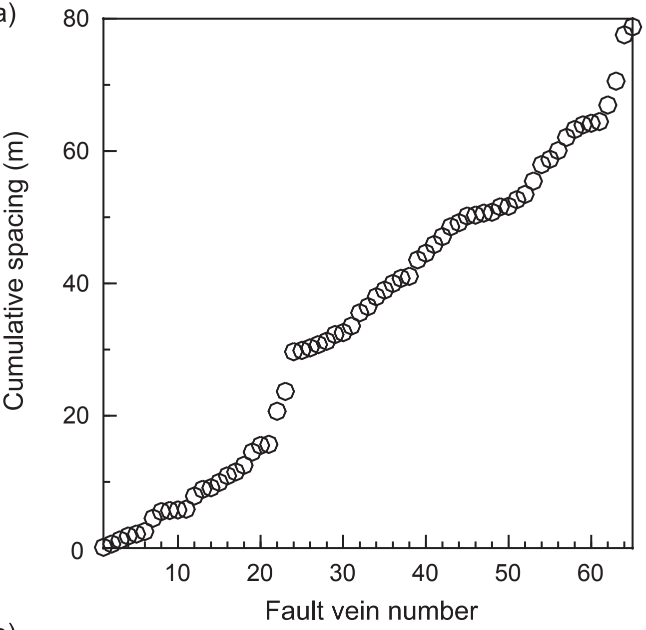
80
60
40
20
0
Cumulative spacing (m)
10
20
30
40
50
60
Fault vein number

b)

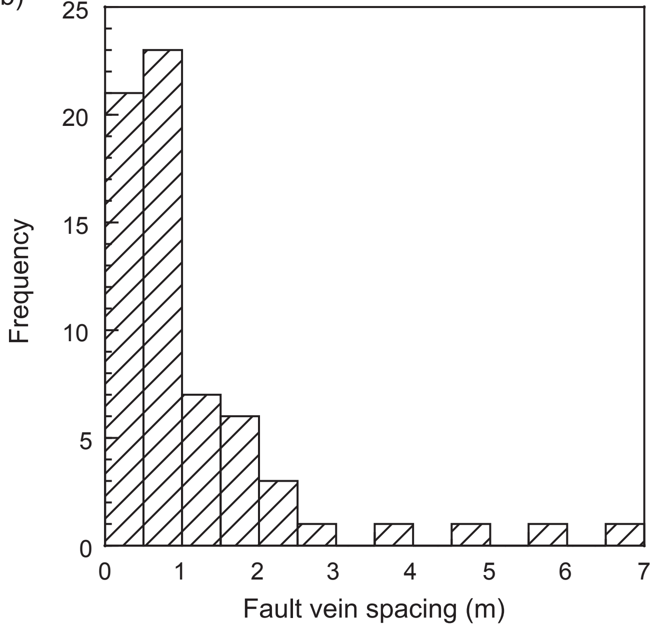
25
20
15
10
5
0
Frequency
0
1
2
3
4
5
6
7
Fault vein spacing (m)

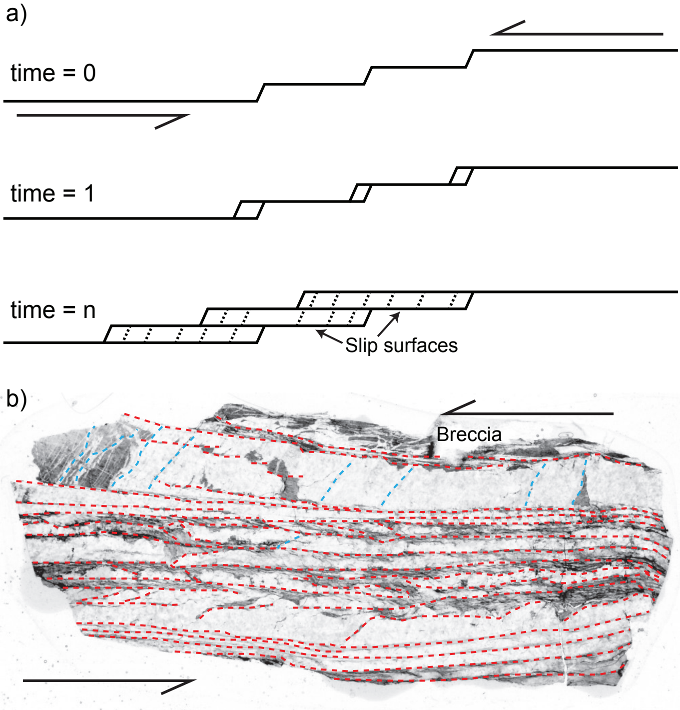

a)
time = 0
time = 1
time = n
Slip surfaces
b)
Breccia

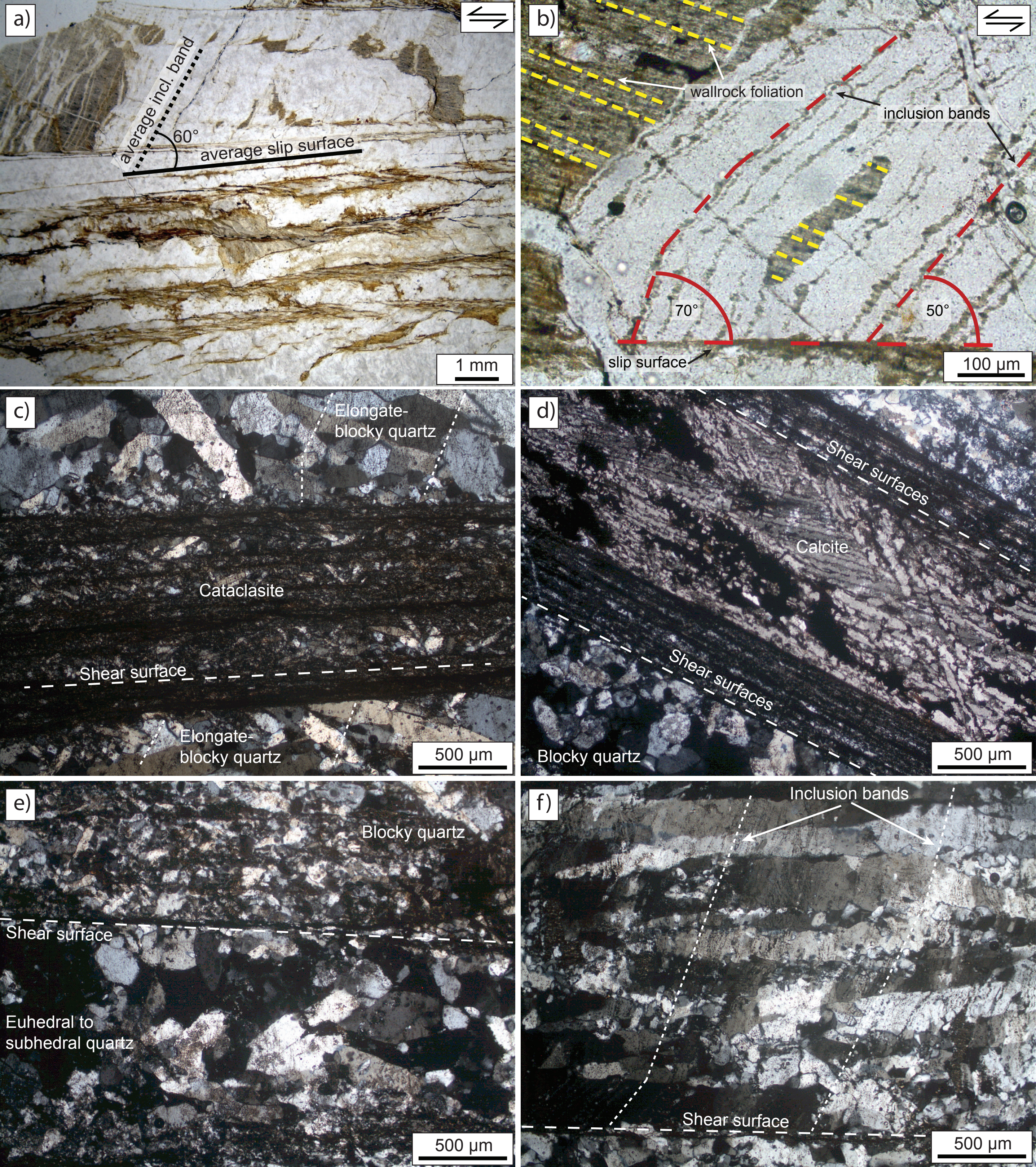

a)
average incl. band
60°
average slip surface
1 mm
b)
wallrock foliation
inclusion bands
70°
50°
slip surface
100 µm
c)
Elongate-
blocky quartz
Cataclasite
Shear surface
Elongate-
blocky quartz
500 µm
d)
Shear surfaces
Calcite
Shear surfaces
Blocky quartz
500 µm
e)
Blocky quartz
Shear surface
Euhedral to
subhedral quartz
500 µm
f)
Inclusion bands
Shear surface
500 µm

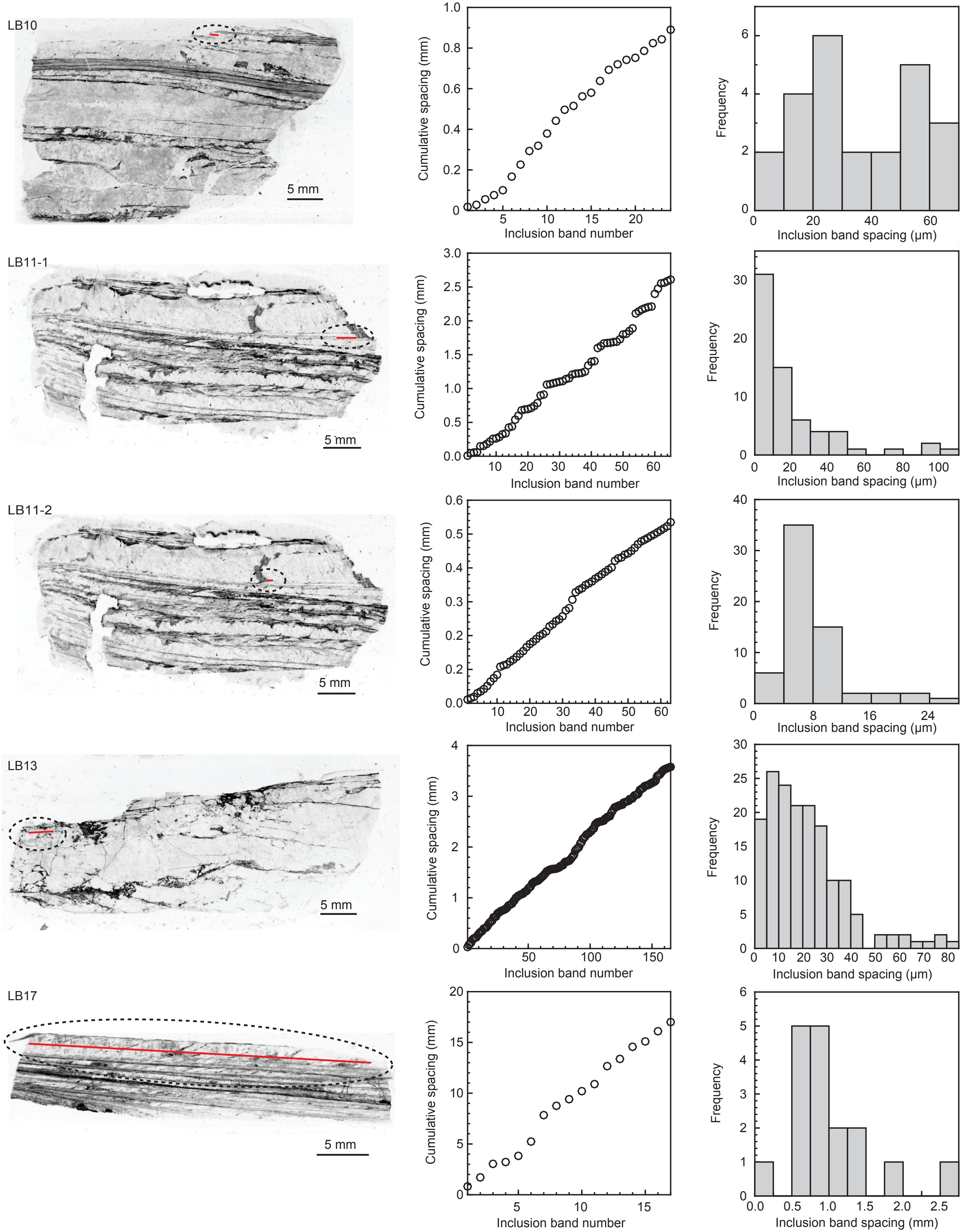

LB10
5 mm
Cumulative spacing (mm)
Inclusion band number
Frequency
Inclusion band spacing (µm)
LB11-1
5 mm
Cumulative spacing (mm)
Inclusion band number
Frequency
Inclusion band spacing (µm)
LB11-2
5 mm
Cumulative spacing (mm)
Inclusion band number
Frequency
Inclusion band spacing (µm)
LB13
5 mm
Cumulative spacing (mm)
Inclusion band number
Frequency
Inclusion band spacing (µm)
LB17
5 mm
Cumulative spacing (mm)
Inclusion band number
Frequency
Inclusion band spacing (mm)

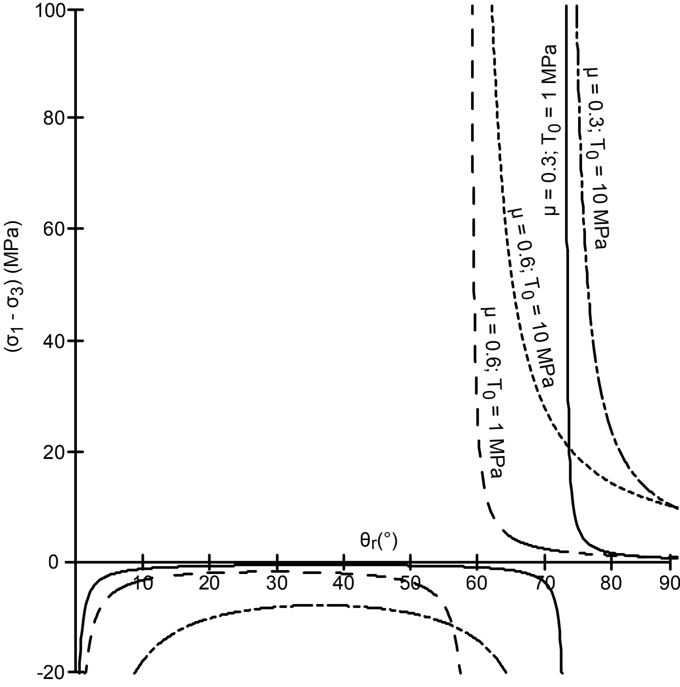

100
80
60
40
20
0
-20
(σ1 - σ3) (MPa)
θr(°)
10
20
30
40
50
60
70
80
90
μ = 0.3; T0 = 1 MPa
μ = 0.3; T0 = 10 MPa
μ = 0.6; T0 = 10 MPa
μ = 0.6; T0 = 1 MPa

Table 1: Statistics of measured spacing between adjacent inclusion bands along transects shown in Figure 8.

Sample	LB10	LB11-1	LB11-2	LB13	LB17
Number of inclusion bands	24	65	63	165	17
Cumulative spacing (mm)	0.89	2.6	0.54	3.6	17
Mean spacing (μm)	37	40	9	22	1000
Standard deviation (μm)	19	47	5	16	555
Minimum spacing (μm)	10	4	3	3	180
Maximum spacing (μm)	67	220	25	82	2600